**Article:**

Bello Garrote, F. L., Sahin, E., Tsunoda, Y. et al. (64 more authors) (2020) $beta$ decay of $^75Ni$ and the systematics of the low-lying level structure of neutron-rich odd-$A$ Cu isotopes. Physical Review C - Nuclear Physics. 034314. ISSN 1089-490X

https://doi.org/10.1103/PhysRevC.102.034314

# $\beta$-decay of $^{75}$Ni and the systematics of the low-lying level structure of neutron-rich odd-A Cu isotopes.

F. L. Bello Garrote,[1] E. Sahin,[1] Y. Tsunoda,[2] T. Otsuka,[2,3,4,5] A. Görgen,[1] M. Niikura,[3] S. Nishimura,[6] G. de Angelis,[7] G. Benzoni,[8] A.I. Morales,[9,8,10] V. Modamio,[1] Z. Y. Xu,[3] H. Baba,[6] F. Browne,[6,11] A.M. Bruce,[11] S. Ceruti,[8] F. Crespi,[8] R. Daido,[12] M.-C. Delattre,[13] P. Doornenbal,[6] Zs. Dombradi,[14] Y. Fang,[12] S. Franchoo,[13] G. Gey,[6,15] A. Gottardo,[7] K. Hadyńska-Klęk,[16] T. Isobe,[6] P.R. John,[17] H.S. Jung,[18] I. Kojouharov,[19] T. Kubo,[6] N. Kurz,[19] I. Kuti,[14] Z. Li,[20] G. Lorusso,[6] I. Matea,[13] K. Matsui,[3] D. Mengoni,[17] T. Miyazaki,[3] S. Momiyama,[3] P. Morfouace,[13] D.R. Napoli,[7] F. Naqvi,[21] H. Nishibata,[12] A. Odahara,[12] R. Orlandi,[22,23] Z. Patel,[6,16] S. Rice,[6,16] H. Sakurai,[3,6] H. Schaffner,[19] L. Sinclair,[6,24] P.-A. Söderström,[6] D. Sohler,[14] I.G. Stefan,[13] T. Sumikama,[25] D. Suzuki,[13] R. Taniuchi,[3] J. Taprogge,[6,26,27] Zs. Vajta,[6,14] J.J. Valiente-Dobón,[7] H. Watanabe,[28] V. Werner,[21,29] J. Wu,[6,20] A. Yagi,[12] M. Yalcinkaya,[30] R. Yokoyama,[3] and K. Yoshinaga[31]

[1] *University of Oslo, Department of Physics, N-0316 Oslo, Norway*
[2] *Center for Nuclear Study, University of Tokyo, Hongo, Bunkyo-ku, Tokyo 113-0033, Japan*
[3] *Department of Physics, University of Tokyo, 7-3-1 Hongo, Bunkyo, Tokyo 113-0033, Japan*
[4] *National Superconducting Cyclotron Laboratory, Michigan State University, East Lansing, Michigan 48824, USA*
[5] *Instituut voor Kern- en Stralingsfysica, KU Leuven, B-3001 Leuven, Belgium*
[6] *RIKEN Nishina Center, 2-1 Hirosawa, Wako, Saitama 351-0198, Japan*
[7] *Istituto Nazionale di Fisica Nucleare, Laboratori Nazionali di Legnaro, I-35020 Legnaro, Italy*
[8] *Istituto Nazionale di Fisica Nucleare, Sezione di Milano, Via Celoria 16, 20133 Milano, Italy*
[9] *Dipartimento di Fisica dell'Università degli Studi di Milano, Via Celoria 16, 20133 Milano, Italy*
[10] *IFIC, CSIC-Universitat de València, E-46071 València, Spain*
[11] *School of Computing, Engineering and Mathematics, University of Brighton, Brighton, BN2 4GJ, UK*
[12] *Department of Physics, Osaka University, 1-1 Machikaneyama, Toyonaka, Osaka 560-0043, Japan*
[13] *Institut de Physique Nucleaire (IPN), IN2P3-CNRS, Universite Paris-Sud 11, F-91406 Orsay Cedex, France*
[14] *Institute for Nuclear Research of the Hungarian Academy of Sciences, Debrecen H-4001, Hungary*
[15] *LPSC, Universite Joseph Fourier Grenoble 1, CNRS/IN2P3, Institut National Polytechnique de Grenoble, F-38026 Grenoble Cedex, France*
[16] *Department of Physics, University of Surrey, Guildford GU2 7XH, United Kingdom*
[17] *INFN Sezione di Padova and Dipartimento di Fisica e Astronomia, Università di Padova, Padova, Italy*
[18] *Department of Physics, University of Notre Dame, Notre Dame, Indiana 46556, USA*
[19] *GSI Helmholtzzentrum für Schwerionenforschung GmbH, 64291 Darmstadt, Germany*
[20] *Department of Physics, Peking University, Beijing 100871, China*
[21] *Wright Nuclear Structure Laboratory,Yale University, New Haven, CT 06520-8120, US*
[22] *Instituut voor Kern- en StralingsFysica, K.U. Leuven, B-3001 Heverlee, Belgium*
[23] *Advanced Science Research Center, JAEA, Tokai, Ibaraki 319-1195, Japan*
[24] *Department of Physics, University of York, Heslington, York YO10 5DD, United Kingdom*
[25] *Department of Physics, Tohoku University, 6-3 Aramaki-Aoba, Aoba, Sendai 980-8578, Japan*
[26] *Departamento de Fsica Teorica, Universidad Autonoma de Madrid, E-28049 Madrid, Spain*
[27] *Instituto de Estructura de la Materia, CSIC, E-28006 Madrid, Spain*
[28] *International Research Center for Nuclei and Particles in the Cosmos, Beihang University, Beijing 100191, China*
[29] *Institut für Kernphysik, TU Darmstadt, 64289 Darmstadt, Germany*
[30] *Department of Physics, Faculty of Science, Istanbul University, Vezneciler/Fatih, 34134, Istanbul, Turkey*
[31] *Department of Physics, Tokyo University of Science, 2641 Yamazaki, Noda, Chiba 278-8510, Japan*

(Dated: July 15, 2019)

**Background:** Detailed spectroscopy of neutron-rich odd-A Cu isotopes is of great importance for studying the shell evolution in the region of $^{78}$Ni. While there is experimental information on excited states in $^{69-73,77,79}$Cu isotopes, the information concerning $^{75}$Cu is very limited.

**Purpose:** Experimentally observed single-particle, core-coupling, and proton-hole intruder states in $^{75}$Cu, will complete the systematics of these states in the chain of isotopes.

**Method:** Excited states in $^{75}$Cu were populated in the $\beta$-decay of $^{75}$Ni isotopes. The Ni nuclei were produced by the in-flight fission of $^{238}$U projectiles, and were separated, identified, and implanted in a highly segmented Si detector array for the detection of the $\beta$-decay electrons. The $\beta$-delayed $\gamma$ rays were detected in a HPGe cluster array. Monte Carlo shell model calculations were performed using the A3DA interaction built on the $pfg_{9/2}d_{5/2}$ model space for both neutrons and protons.

**Results:** A level scheme of $^{75}$Cu was built up to ∼4 MeV by performing a $\gamma$-$\gamma$ coincidence analysis. The excited states below 2 MeV were interpreted based on the systematics of neutron rich odd-A Cu isotopes and the results of the shell model calculations.

**Conclusions:** The evolution of the single-particle, core-coupling, and proton-hole intruder states in the chain of neutron-rich odd-A Cu isotopes is discussed in the present work, in connection with the newly observed level structure of $^{75}$Cu.

## I. INTRODUCTION

The shell structure of exotic nuclei towards the driplines is expected to differ from that of stable nuclei. Theoretical predictions and existing experimental data so far indicate that the nuclear shell structure, now recognized as a more local than global concept within the nuclear chart, is not as robust as previously thought [1]; the weakening of the spherical shell gaps has been shown to be closely related to the tensor component of the monopole shell-model Hamiltonian [2, 3]. The region near the doubly-magic nucleus $^{78}$Ni, with its very large neutron-to-proton ratio, is of great interest for shell evolution studies, but continues to be, at the moment, very difficult to investigate experimentally. Here, the systematic study of the excited states of neutron-rich, odd-A Cu isotopes from $A = 69$ to 79 plays a vital role in understanding the structural changes between the $N = 40$ sub-shell and $N = 50$ shell closures. Shell-model calculations find modifications of the proton single-particle energies in the Ni chain with increasing the number of neutrons in the $\nu 1g_{9/2}$ orbital, leading to the inversion of the $\pi 2p_{3/2}$ and $\pi 1f_{5/2}$ orbitals [2–4]. This was confirmed by measuring the inversion of the $3/2^-$ and $5/2^-$ states in the neutron-rich odd-A Cu isotopes [5, 6]. After considering the experimentally available information on excited states in $^{77}$Cu, the size of the $Z = 28$ shell gap was found to be reduced to approximately 5 MeV at $N = 50$ [7].

Spectroscopic information on the low-lying states in $^{69-73}$Cu has been obtained in $\beta$-decay [8], Coulomb excitation [9], and lifetime-measurement experiments [10]. In $^{69,71}$Cu, higher spin states are known from fragmentation [11] and multi-nucleon transfer reactions [12–15]. In $^{77}$Cu, excited states were populated in the $\beta$-decay of $^{77}$Ni [7] and in the single proton knock-out of $^{78}$Zn [16]. In $^{79}$Cu, excited states up to ∼ 4.5 MeV have been observed for the first time in a proton knockout reaction [17]. In $^{75}$Cu, previous to the present work, only two low-lying isomeric states had been reported from fragmentation reactions [18–20]. The level scheme obtained in the present $\beta$-decay study fills the gap in the systematics of the neutron-rich, odd-A Cu isotopes, providing a more complete picture for studying the shell evolution in the region of $^{78}$Ni. In parallel with the present work, results from a proton knockout experiment on $^{75}$Cu and $^{77}$Cu are presented [21], establishing the nature of some of the observed states in these isotopes.

## II. EXPERIMENTAL SETUP

The data presented in this work originates from separate experiments performed during the EURICA campaign [22] at the Radioactive Ion Beam Factory (RIBF) [23] of the RIKEN Nishina Center. A primary beam of $^{238}$U with 345$A$ MeV energy was delivered by the RIKEN accelerator complex [24] with an average intensity of 10 pnA. Short-lived, neutron-rich nuclides were produced by in-flight fission of the $^{238}$U projectiles on a $^{9}$Be target with 555 mg/cm$^2$ thickness. Fragments of interest were selected in the first part of the BigRIPS fragment separator [25] using the B$\rho$-ΔE-B$\rho$ method [26]. These experiments aimed at studying nuclei in the region near $^{78}$Ni and used very similar settings of the BigRIPS separator for the selection of the fragments [27]. The particle identification (PID) was performed using the TOF-B$\rho$-ΔE method [28], making use of the beam-line detectors both in the second half of BigRIPS and in the ZeroDegree spectrometer [25]. A PID plot from the experiments can be found in Ref. [29]. The $^{75}$Ni ions were transmitted to the detection system, where their $\beta$-decay to $^{75}$Cu and subsequent $\gamma$ decay was detected.

The secondary beam of radioactive ions was implanted into the wide-range active silicon strip stopper array for beta and ion detection (WAS3ABi) [30], which consisted of a stack of 8 DSSSD detectors located at the last focal point (F11) of the ZeroDegree spectrometer. Each DSSSD had 60 horizontal and 40 vertical strips of 1 mm pitch, respectively, giving a total of 2400 1x1 mm$^2$ pixels in each detector. The DSSSDs had a thickness of 1 mm and were separated in depth by 0.5 mm. The velocity of the fragments was reduced by an aluminum degrader located in front of WAS3ABi to ensure the implantation of the desired fragments in the center of the stack. A timestamp value was recorded for all the implantation and $\beta$-decay events detected in WAS3ABi. The EUROBALL-RIKEN Cluster Array (EURICA) of germanium detectors [22] was surrounding WAS3ABi with the purpose of detecting $\beta$-delayed $\gamma$ rays. The average absolute photo-peak efficiency of the EURICA array during the experiments was ∼6.5% at 1.33 MeV.

## III. DATA ANALYSIS AND EXPERIMENTAL RESULTS

The incoming $^{75}$Ni ions were correlated in time with implantation events and subsequent $\beta$-decay electrons detected in WAS3ABi. To correlate the $\beta$-decay signals with the implanted $^{75}$Ni ions it was required that they originated from the same DSSSD within a correlation

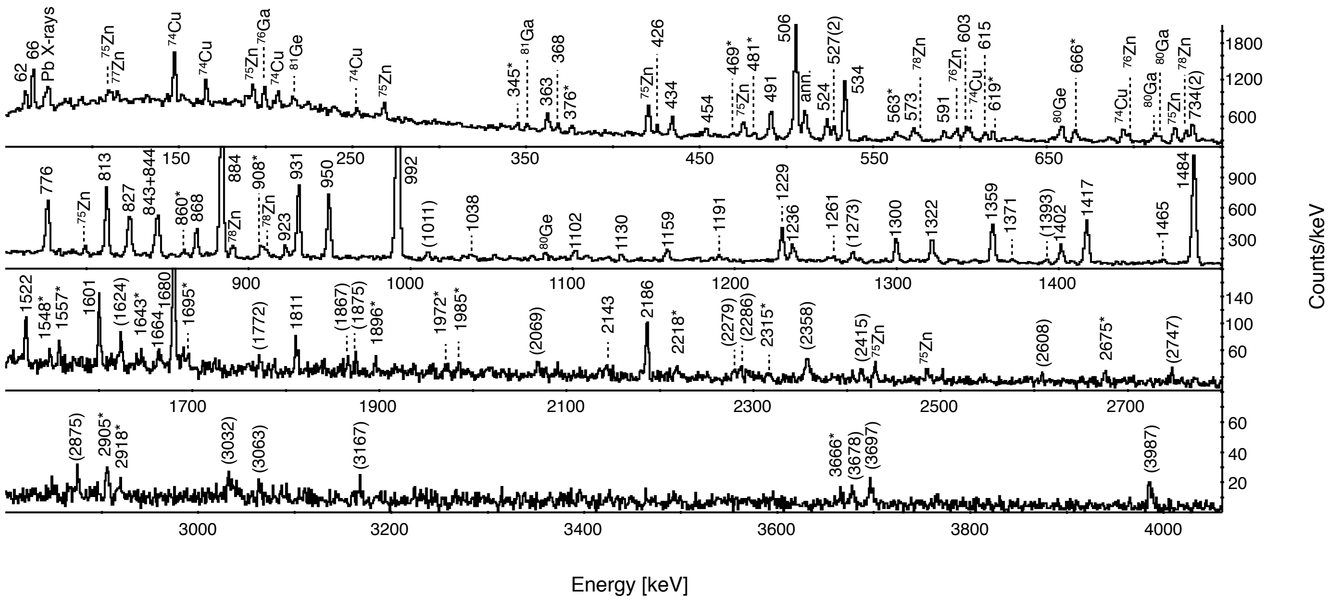


FIG. 1. Singles spectrum of $\gamma$ rays measured in coincidence with the first position-correlated electrons detected within 2.5 s after the implantation of $^{75}$Ni ions. Transitions labeled by their energy only, were assigned to $^{75}$Cu and have been placed in the level scheme of Fig. 5. Transitions labeled by their energy in parentheses were tentatively assigned to $^{75}$Cu, but could not be placed in the level scheme due to insufficient coincidence relations. Transitions identified to originate from isotopes other than $^{75}$Cu are labeled with the respective symbol of the nuclide. Transitions that could not be assigned to any specific nuclide are labeled with their energy followed by an asterisk ($\star$).

area that covered up to two pixels away from the implantation position. Figure 1 shows the $\gamma$-ray singles spectrum in coincidence with the first position-correlated electrons detected within 2.5 s after the implantation of the $^{75}$Ni ions (7.5 times the half-live of $^{75}$Ni [29]). Most of the observed transitions can be expected to originate from excited states in $^{75}$Cu, but transitions from other nuclides may be present in the singles spectrum. Excited states in $^{74}$Cu are populated by $\beta$-delayed neutron emission with a reported probability of 10.0(28)% [31]. Although the level scheme for $^{74}$Cu is completely unknown, the origin of the strongest transitions following beta-delayed neutron emission could be confirmed by gating on the $^{74}$Ni ions ($1.47 \times 10^5$) implanted during the experiments. In cases where the electron from the $\beta$-decay of $^{75}$Ni to $^{75}$Cu escaped detection, the correlated electron can originate from the daughter decay from $^{75}$Cu to $^{75}$Zn, leading to a contamination of the spectrum with $\gamma$ rays from $^{75}$Zn.

Finally, there are transitions in the spectrum due to random coincidences with beta-decay events from isotopes such as $^{77,78}$Cu or $^{80,81}$Zn that were implanted with high rates. It was possible to identify such contaminant lines by looking at $\gamma$-ray spectra in coincidence with electrons that were detected inside the correlation area, but outside the time window of 2.5 s after implantation. Transitions in $^{75}$Cu were strongly suppressed in the spectra recorded between 0.5 and 1.5 s before, and between 2.5 and 5 s after implantation of the $^{75}$Ni ions, whereas transitions originating from random coincidences and the daughter decays, respectively, were enhanced. All transitions which were identified as originating from nuclides other than $^{75}$Cu are labeled in Fig. 1 with the corresponding symbol of the nuclide. Those transitions which were identified as contaminants, but could not be associated with any specific nuclide are labeled with their energy followed by an asterisk ($\star$). All the other transitions were assigned to $^{75}$Cu and labeled with their energy. Those transitions in $^{75}$Cu that could be firmly placed in the level scheme (Fig. 5) are labeled without parentheses, whereas those that could not be placed in the level scheme due to insufficient coincidence relations are labeled by their energies in parentheses. The energies and absolute intensities of the transitions assigned to $^{75}$Cu are listed in Table I.

The number of $\beta$-decay events of $^{75}$Ni recorded during the experiment can be obtained by evaluating the total decay curve using known parameters for the subsequent decays of the daughter and granddaughter nuclides. The total decay curve with fits of the individual decays is shown in Fig. 2. The decay curve shows the time difference between the implantation of the $^{75}$Ni ions and the detection of electrons inside the area of correlation, within a time window of 5 s. The constant background was obtained from electron events that were recorded between 1.5 and 0.5 s before the implantation events. To build the total decay curve, not only the first, but all the electrons detected after the implantation were con-

TABLE I. Energies ($E_\gamma$) and absolute intensities ($I_\gamma$) of the $\gamma$-ray transitions assigned to $^{75}$Cu. For those transitions placed in the level scheme of Fig. 5, the initial states ($E_i$) are indicated. Transitions that could not be placed in the level scheme are given in parentheses. The intensities of the 61.8 and 66.2 keV isomeric transitions were corrected for the finite size of the time window that was set for the collection of the $\gamma$ rays. The intensities are corrected for internal conversion, using conversion coefficients calculated from Ref. [33].

| $E_\gamma$ [keV] [a] | $E_i$ [keV][a] | $I_\gamma$ [%] | $E_\gamma$ [keV][a] | $E_i$ [keV][a] | $I_\gamma$ [%] | $E_\gamma$ [keV][a] | $E_i$ [keV][a] | $I_\gamma$ [%] | $E_\gamma$ [keV][a] | $E_i$ [keV][a] | $I_\gamma$ [%] |
|---|---|---|---|---|---|---|---|---|---|---|---|
| 61.8 | 61.8 | 12.6(38) | 734.1[d] | 2414.5 | 0.81(56) | 1236.1 | 2228.3 | 2.06(14) | (1866.5) | | <0.3 |
| 66.2 | 66.2 | 10.0(20)[b] | 776.2 | 1726.1 | 4.99(18) | 1261.2 | 2253.3 | 0.70(11) | (1874.9) | | 0.31(11) |
| | | 2.99(58)[c] | 812.6 | 3227.1 | 5.79(20) | (1273.1) | | 1.04(12) | (2069.4) | | <0.3 |
| 362.5 | 2351.6 | 1.92(17) | 826.7 | 1819.0 | 5.02(19) | 1299.9 | 2351.6 | 2.46(14) | 2142.8 | 3135.9 | 0.50(11) |
| 368.4 | 2357.4 | 0.74(13) | 842.8[d] | 3194.4 | 2.12(50) | 1322.1 | 2805.4 | 2.71(16) | 2186.1 | 3135.9 | 1.81(16) |
| 425.5 | 2414.5 | 0.71(13) | 844.3[d] | 2833.3 | 2.89(47) | 1359.4 | 2351.6 | 5.24(20) | (2279.4) | | <0.3 |
| 434.2 | 2253.3 | 1.61(15) | 868.1 | 2351.6 | 2.64(15) | 1371.4 | 3963.9 | 0.58(14) | (2286.1) | | <0.3 |
| 453.7 | 2805.4 | 1.35(14) | 883.6 | 949.7 | 15.64(37) | (1392.7) | | 0.48(9) | (2357.7) | | 0.77(11) |
| 491.1 | 1483.5 | 3.58(17) | 923.1 | 3750.6 | 0.79(10) | 1401.7 | 2351.6 | 2.54(15) | (2415.3) | | <0.3 |
| 505.5 | 1989.0 | 13.45(29) | 931.0 | 2414.5 | 6.23(20) | 1417.4 | 1483.5 | 5.48(21) | (2608.4) | | <0.3 |
| 523.5 | 3750.6 | 2.82(15) | 949.8 | 949.7 | 5.64(18) | 1464.8 | 2414.5 | 0.32(9) | (2747.3) | | <0.3 |
| 527.3[d] | 2253.3 | 0.63(33) | 992.2 | 992.2 | 26.24(55) | 1483.6 | 1483.5 | 14.33(41) | (2874.9) | | <0.3 |
| 527.3[d] | 2516.3 | 0.87(30) | (1010.8) | | 0.98(13) | 1522.0 | 3775.3 | 1.16(13) | (3032.1) | | 0.43(11) |
| 533.7 | 1483.5 | 6.96(21) | 1037.8 | 3750.6 | 0.60(14) | 1600.5 | 2592.5 | 1.47(13) | (3063.4) | | <0.3 |
| 573.2 | 2924.8 | 3.10(18) | 1101.5 | 2827.5 | 1.00(12) | (1623.9) | | 0.75(11) | (3167.2) | | <0.3 |
| 590.9 | 3005.4 | 2.14(15) | 1130.4 | 3963.9 | 0.58(10) | 1664.0 | 3651.5 | 0.47(12) | (3677.7) | | 0.32(8) |
| 603.1 | 2592.5 | 2.14(18) | 1158.6 | 3963.9 | 1.43(13) | 1680.4 | 1680.4 | 4.22(21) | (3697.1) | | 0.30(8) |
| 614.5 | 3750.6 | 2.23(15) | 1190.5 | 2674.0 | 0.58(11) | (1772.3) | | 0.34(10) | (3986.7) | | 0.51(9) |
| 734.1[d] | 1726.1 | 1.22(49) | 1229.4 | 2712.9 | 3.57(16) | 1811.3 | 2805.4 | 1.06(13) | | | |

[a] Uncertainties are within 1 keV
[b] Assuming pure $E2$ multipolarity
[c] Assuming pure $M1$ multipolarity
[d] Doublet

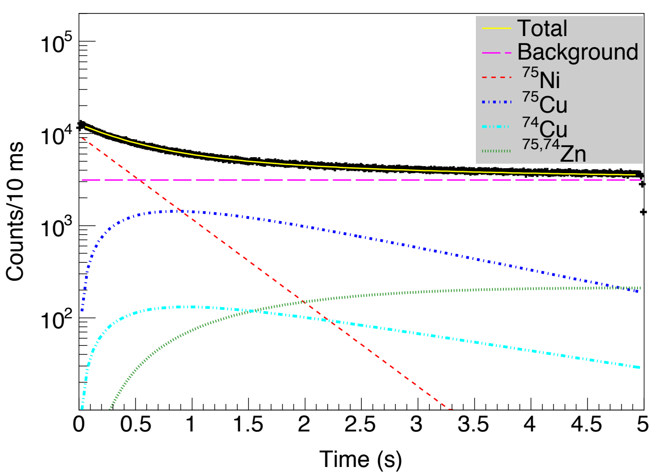


FIG. 2. (Color online) Time difference between implantation of $^{75}$Ni ions and detection of electrons inside the area of spatial correlation. The various curves show the fit of contributions from individual decays based on known half-lives and probability for beta-delayed neutron emission (see text for more details).

sidered. Evaluated half-lives for $^{75,74}$Cu and $^{75,74}$Zn [32] and the reported $\beta$-delayed neutron emission probability for $^{75}$Ni [31] were used as fixed parameters in the fit. The half-life of $^{75}$Ni, $T_{1/2} = 331.6(32)$ ms, was obtained from the present experimental data by gating on the 992, 884 and 1484 keV transitions [27, 29]. A total number of $4.53(3)\times10^5$ $^{75}$Ni $\beta$-decays in a time window of 2.5 s after implantation of the ions was obtained after removing all contributions from background and subsequent decays. The method for fitting the decay curve is explained in more detail in Ref. [27].

The quality and amount of data allowed performing a $\gamma$-$\gamma$ coincidence analysis. Figure 3 shows background-subtracted $\gamma$-ray spectra gated on the four strongest transitions of 992, 884, 1484 and 506 keV. The level scheme shown in Fig. 5 was constructed based on coincidence relations between the transitions, their energy sums and differences, and their intensities. From the intensities of the transitions, log $ft$ values were obtained using $T_{1/2} = 331.6(32)$ ms [27, 29] and $Q_{\beta^-} = 10230(300)$ keV [34]. A total of 71.6(35)% of the $\beta$-decay events were found to feed the excited states of $^{75}$Cu that are included in the level scheme of Fig. 5, while 11.6(3)% of the events were found to feed excited states of $^{74}$Cu trough the emission of $\beta$-delayed neutrons. The latter value can only be considered a lower limit for the $\beta$-delayed neutron emission probability, because the $\beta$-delayed neutron branch feeding the ground state of $^{74}$Cu is unknown. Based on these values, a maximum of 20.6% of $\beta$-decay intensity could directly feed the ground states in $^{75}$Cu or $^{74}$Cu.

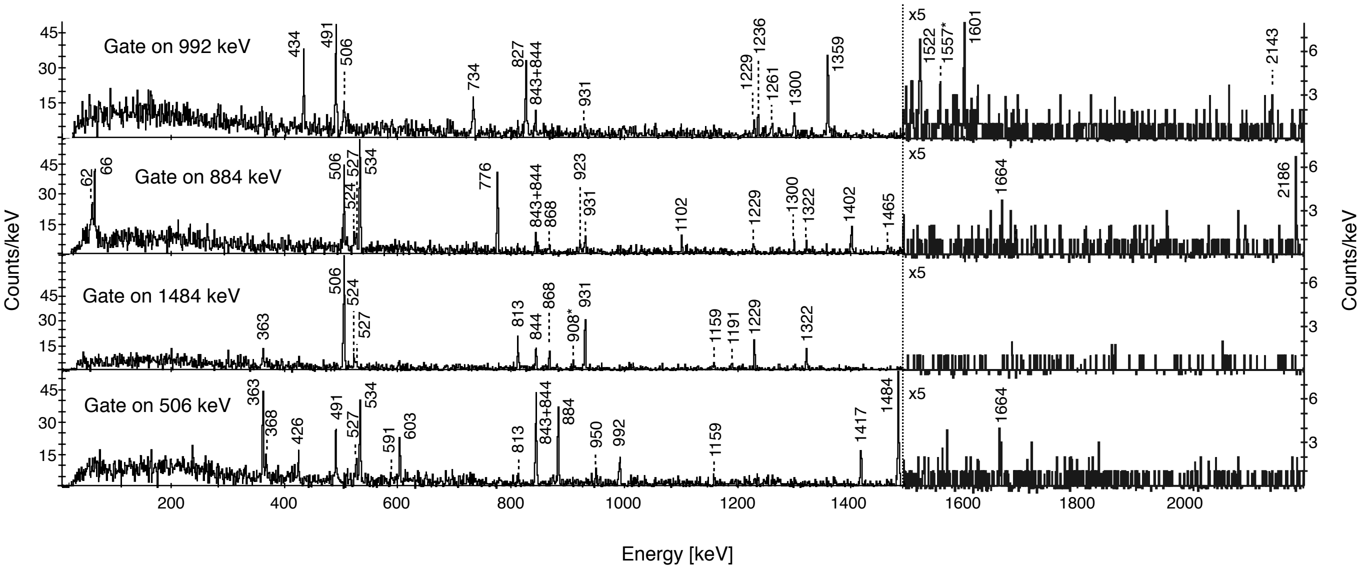


FIG. 3. Background-subtracted $\gamma$-ray spectra gated on the four strongest transitions of $^{75}$Cu with energies 992, 884, 1484, and 506 keV. All transitions which are labeled by their energy have been placed in the level scheme of Fig. 5, except those at 908 and 1557 keV (labeled by $\star$).

A further 9.3(10)% of the absolute $\gamma$-ray intensity was tentatively assigned to $^{75}$Cu, but could not be placed in the level scheme (see Table I). If it is assumed that all these unplaced transitions directly feed the ground state of $^{75}$Cu, the unobserved $\beta$-decay feeding decreases to 8(4)%.

The spin assignments in Fig. 5 are based on the known $5/2^-$ ground-state spin-parity of $^{75}$Cu [5, 6] and the possible multipolarities of the $\gamma$-ray transitions, the systematics of the odd-A Cu isotopes between $^{69}$Cu and $^{79}$Cu, and the comparison with theoretical calculations, which will be discussed in Section IV. The only exception is the $7/2^-$ state at 1680 keV, for which the spin and parity assignment was mostly based on the results of the shell model calculations (see Sec. IV C). All the excited states with assigned spin values were assigned a negative parity. Although the measured log *ft* values can not be used as a firm criterion to perform spin and parity assignments (because of the large systematic error in the $\beta$-decay branching ratios related to the unplaced $\beta$-decay intensity), those states with log *ft* values which are only consistent with allowed decays (log $ft < 6$), appear above 2.5 MeV, suggesting the occurrence of positive-parity states at these energies, in agreement with the systematics [8, 35].

The time window for the $\beta$-$\gamma$ coincidences was sufficiently long to observe the previously known isomeric 61.8 and 66.2 keV transitions with half-lives of 310(8) and 149(6) ns, respectively [18, 19], in coincidence with other transitions. Figure 4 shows the low-energy part of the background-subtracted $\gamma$-ray spectra gated on the 884, 950, 1417, and 1484 keV transitions. The presence of lines at 61.8 and 66.2 keV in the spectra gated on the 884 and 1417 keV transitions, together with their non-observation in the spectra gated on the 950 and 1484 keV transitions, respectively, fixes the positions of the 61.8 and 66.2 keV states, in agreement with the more recent works in Refs. [19, 20] and in disagreement with the earlier work in Ref. [18]. It should be noticed that the energy difference between the 950 and the 884 keV transitions and between the 1484 and the 1417 keV transitions matches the energy of the 66.2 keV transition.

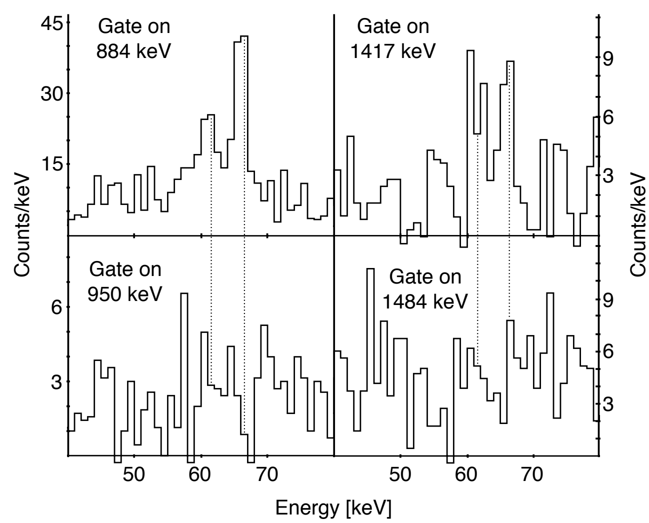


FIG. 4. Background-subtracted $\gamma$-ray spectra gated on the 884, 950, 1417, and 1484 keV transitions in the energy range of the two isomeric transitions of 61.8 and 66.2 keV.

The fact that the 884 and the 1417 keV transitions are

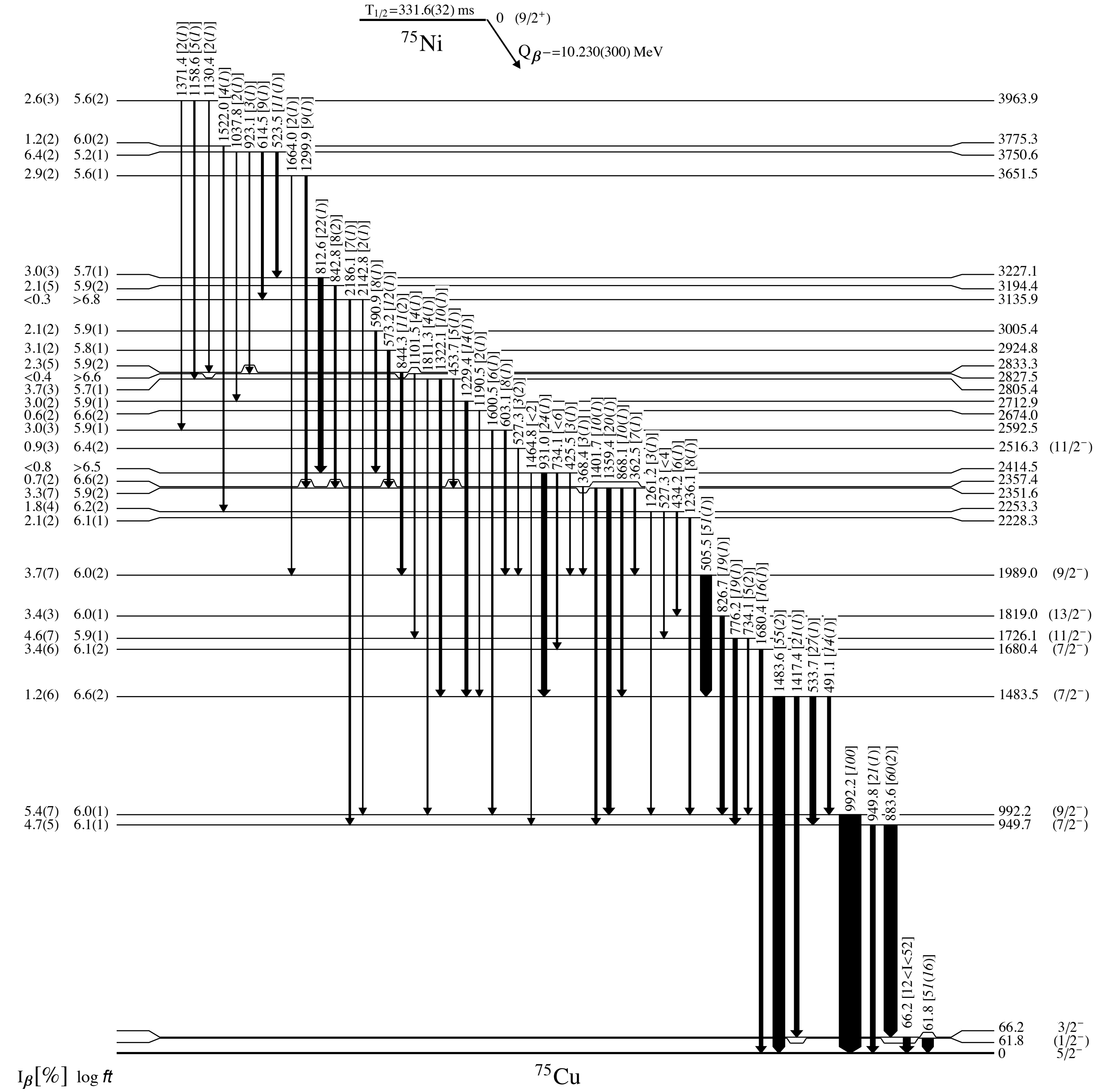


FIG. 5. Level scheme of $^{75}$Cu. The energies of the states and the transitions are given in keV, and the uncertainties are within 1 keV. The relative intensities of the transitions (in brackets) are normalized to the 992 keV transition and corrected for internal conversion. Lower and upper limits are given for the relative intensity of the 66.2 keV transition. For the discussion of the $\beta$-decay branching ratios ($I_\beta$) to the 61.8 and 66.2 keV states, and to the ground state, see the text (Section III).

in coincidence with the 61.8 keV transition, implies the existence of an intense low-energy transition of 4.4(6) keV connecting the two isomers, which was already discussed by Petrone *et al.* [19]. Without any isomeric states reported for the parent nucleus $^{75}$Ni, all $\beta$-decays are assumed to originate from its ground state, which has a proposed $9/2^+$ spin and parity. Therefore, based on the proposed spin and parities of the isomers, (see Section IV), there should be no direct $\beta$-decay feeding of these states. Since no direct $\gamma$-ray feeding of the state at 61.8 keV excitation energy was observed, all feeding into this 61.8 keV state should therefore proceed through the 4.4 keV transition. The absence of direct $\beta$-decay feeding of these states could not be experimentally confirmed due to the large uncertainties for the intensities of the 61.8 and 66.2 keV transitions and the non-observation of the 4.4 keV transition.

## IV. DISCUSSION

In the low-lying level structure of odd-mass Cu isotopes, which in a normal occupation scheme have only one proton outside the $Z = 28$ shell gap, the occupation of the $1f_{5/2}$, $2p_{3/2}$, or $2p_{1/2}$ orbitals by the unpaired proton will give rise to $5/2^-$, $3/2^-$, and $1/2^-$ states with single-particle nature. The same proton above the $Z = 28$ shell gap could also couple to excited states in the corresponding even-even Ni cores, creating particle-core coupled multiplets. Furthermore, the presence of $7/2^-$ states with proton-hole $1f_{7/2}^{-1}$ configurations at relatively low energies, could be favored in isotopes with $N \geq 40$ because of the reduction of the $Z = 28$ shell gap with the filling of the $\nu 1g_{9/2}$ orbital, and the occurrence of quadrupole correlations between excited protons and $\nu 1g_{9/2}$ neutrons [2, 4, 7, 36–38]. In the following sections, the low-lying level structure of $^{75}$Cu is discussed in the context of the systematics of the $N \geq 40$ odd-mass Cu isotopes.

To help identifying the populated low-lying states, and to better understand the level structure of $^{75}$Cu, Monte Carlo shell model (MCSM) calculations were performed in the present work. The MCSM calculations used the A3DA interaction [37, 39], which is built on the $pfg_{9/2}d_{5/2}$ model space for both neutrons and protons, assuming $^{40}$Ca as inert core. Those experimental energy states with assigned spin and parity are shown in Fig. 6 together with the corresponding calculated energy states. The agreement with the experimental levels is good. For each of these states, occupation numbers are shown in Table II. The composition of their wave function was evaluated in terms of the probability of coupling one proton in the $1f_{7/2}$, $1f_{5/2}$, $2p_{3/2}$, or $2p_{1/2}$ orbitals to different energy states in the $^{74}$Ni core. $B(E2, M1)$ values, electric quadrupole, and magnetic moments were calculated. Furthermore, the shapes of the MCSM basis vectors for each state were calculated, and are shown in Fig. 7 together with the potential energy surface (PES) of the nucleus. Some of the results from the MCSM calculations have been previously reported for $^{75}$Cu [20] , $^{77}$Cu [7] and $^{79}$Cu [17]. Occupation numbers corresponding to excited states in $^{77}$Cu are shown in Table III.

### A. The $5/2^-$, $3/2^-$ and $1/2^-$ states.

The first $5/2^-$ and $3/2^-$ states in odd-mass Cu isotopes with $N \geq 40$ have been associated with $\pi 1f_{5/2}$ and $\pi 2p_{3/2}$ single-particle configurations, respectivly [7, 8, 17]. The predominant single-particle character of these states in $^{69-73}$Cu was indicated by measuring relatively

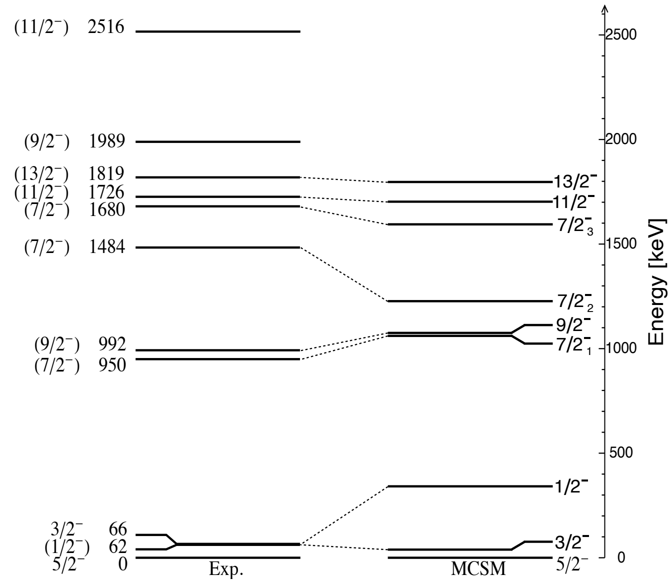


FIG. 6. (left): Experimental energy states of $^{75}$Cu with assigned spins and parities. (right): MCSM calculations.

low $B(E2; 5/2^- \rightarrow 3/2^-_{gs})$ values (<5 W.u.) [9]. Spectroscopic factors measured in (d,$^3$He) and ($\vec{t}$,$\alpha$) reactions [40–43] established the spin and parity of the $5/2^-$ states in $^{69,71}$Cu, and confirmed the $\pi 1f_{5/2}$ and $\pi 2p_{3/2}$ single-particle character of the $5/2^-$ states and the $3/2^-$ ground states, respectively. The significant deviations from the effective Schmidt estimates of the magnetic mo-

TABLE II. Occupation numbers of proton and neutron orbits of calculated excited states of $^{75}$Cu.

| $J^\pi_n$ | $\pi f_{7/2}$ | $\pi p_{3/2}$ | $\pi f_{5/2}$ | $\pi p_{1/2}$ | $\pi g_{9/2}$ | $\pi d_{5/2}$ |
|---|---|---|---|---|---|---|
| $1/2^-$ | 7.62 | 0.45 | 0.66 | 0.20 | 0.05 | 0.01 |
| $3/2^-$ | 7.65 | 0.86 | 0.35 | 0.08 | 0.06 | 0.01 |
| $5/2^-$ | 7.62 | 0.34 | 0.90 | 0.07 | 0.05 | 0.01 |
| $7/2^-_1$ | 7.64 | 0.77 | 0.43 | 0.10 | 0.06 | 0.01 |
| $7/2^-_2$ | 6.71 | 0.62 | 1.37 | 0.22 | 0.07 | 0.01 |
| $7/2^-_3$ | 7.55 | 0.50 | 0.83 | 0.05 | 0.05 | 0.01 |
| $9/2^-$ | 7.64 | 0.34 | 0.87 | 0.09 | 0.05 | 0.01 |
| $11/2^-$ | 7.66 | 0.83 | 0.36 | 0.08 | 0.06 | 0.01 |
| $13/2^-$ | 7.66 | 0.30 | 0.91 | 0.08 | 0.05 | 0.01 |
| | $\nu f_{7/2}$ | $\nu p_{3/2}$ | $\nu f_{5/2}$ | $\nu p_{1/2}$ | $\nu g_{9/2}$ | $\nu d_{5/2}$ |
| $1/2^-$ | 7.97 | 3.90 | 5.88 | 1.90 | 6.06 | 0.31 |
| $3/2^-$ | 7.97 | 3.88 | 5.85 | 1.89 | 6.21 | 0.21 |
| $5/2^-$ | 7.97 | 3.87 | 5.83 | 1.84 | 6.28 | 0.23 |
| $7/2^-_1$ | 7.97 | 3.92 | 5.91 | 1.93 | 6.01 | 0.26 |
| $7/2^-_2$ | 7.97 | 3.87 | 5.75 | 1.86 | 6.21 | 0.34 |
| $7/2^-_3$ | 7.97 | 3.90 | 5.86 | 1.89 | 6.18 | 0.19 |
| $9/2^-$ | 7.97 | 3.92 | 5.91 | 1.93 | 6.00 | 0.26 |
| $11/2^-$ | 7.97 | 3.93 | 5.94 | 1.95 | 5.96 | 0.24 |
| $13/2^-$ | 7.97 | 3.93 | 5.93 | 1.94 | 5.98 | 0.24 |

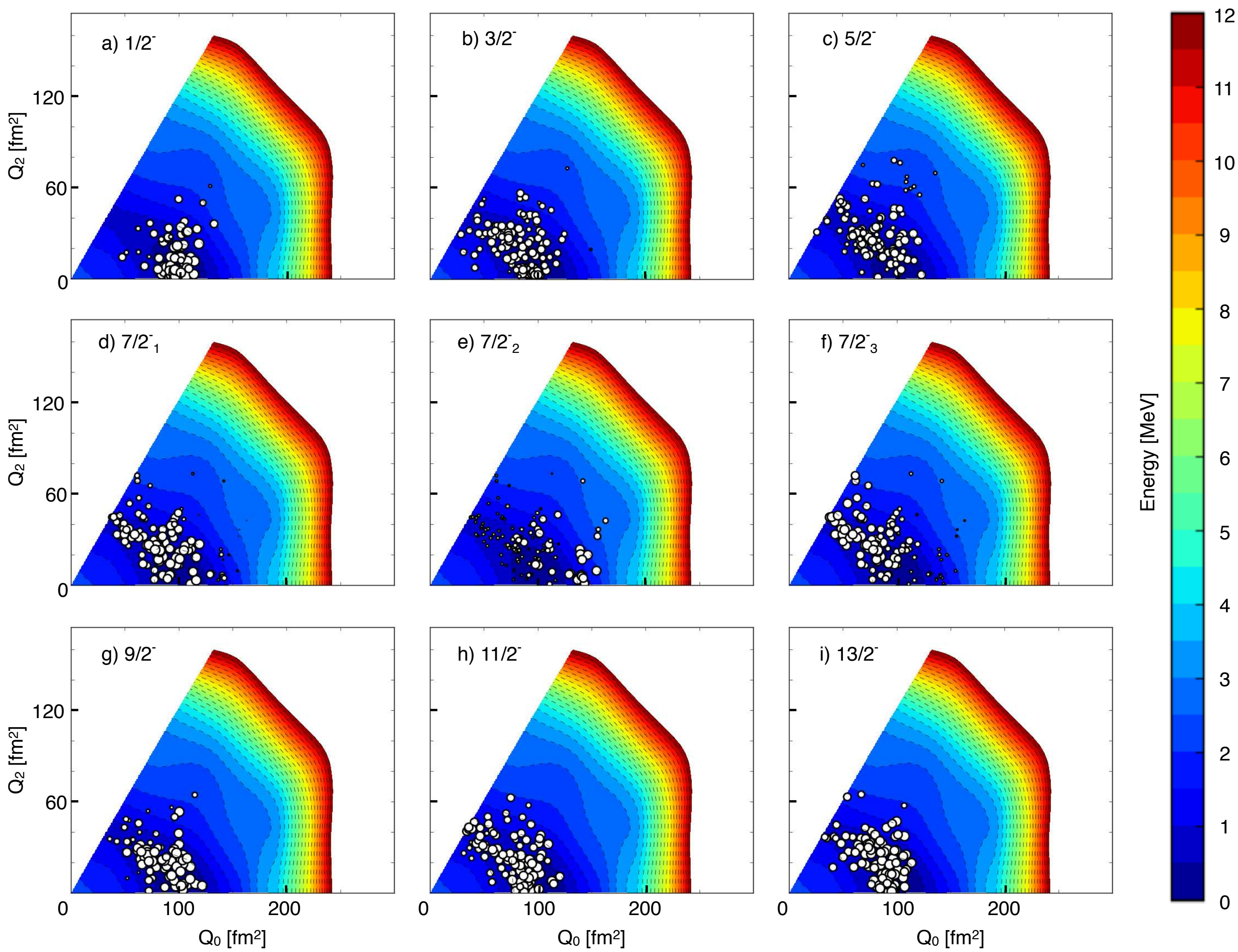


FIG. 7. (Color online) The circles drawn on the potential energy surface of the nucleus indicate the shapes of the MCSM basis vectors of calculated excited states of $^{75}$Cu. See Ref. [37] for details.

ments measured for the ground states in $^{73,75}$Cu [5, 6] and the excited $3/2^-$ state in $^{75}$Cu [20] are interpreted as a consequence of the enhanced collectivity in the $^{72,74}$Ni cores [20].

The systematics of the energies of the first $5/2^-$ and $3/2^-$ states in $^{69-77}$Cu can be seen in Fig. 9. The ground-state spin changes from $3/2^-$ in the lighter isotopes ($A \leq 73$) to $5/2^-$ in the heavier ones [5, 6]. The excited $3/2^-$ state is also know in $^{79}$Cu [17]. In $^{75}$Cu, where the inversion of these energy states occurs, the isomeric $3/2^-$ state lies very close to the ground state [18–20]. The other isomer, at just 4.4 keV below the $3/2^-$ state, has been assigned $1/2^-$ spin and parity, based on systematics of the $1/2^-$ states in the lighter isotopes [18, 19] (see Fig. 8), and the results of the time-differential perturbed angular distribution measurements [20]. In the present $\beta$-decay experiment, no direct $\gamma$-ray feeding of the state at 61.8 keV was observed, while the state at 66.2 keV was directly fed by two transitions with 884 and 1417 keV. This feeding pattern is consistent with spin-parity $3/2^-$ for the state at 66.2 keV, which is fed by $E2$ transitions from $7/2^-$ states above, whereas spin-parity $1/2^-$ for the state at 61.8 keV explains the non-observation of any feeding from higher-spin states due to the high multipolarity that would be required.

The MCSM calculations find the $5/2^-$ ground state and the first $3/2^-$ state of $^{75}$Cu to have a predominant single-particle character, which has been now experimentally verified in Ref. [21] for both $^{75}$Cu and $^{77}$Cu. The $5/2^-$ state is found to have an occupation number of 0.90 in the $\pi 1f_{5/2}$ orbital, and its wave function becomes purer towards the end of the neutron $fp$ shell, with the occupation number increasing to 0.99 in $^{77}$Cu and 1.05 in $^{79}$Cu. The energy of the $3/2^-$ state in $^{75}$Cu is well reproduced by the model (see Fig. 6), and the $B(E2; 3/2^- \rightarrow 5/2^-)$ value was calculated to

TABLE III. Occupation numbers of proton and neutron orbits of calculated excited states of $^{77}$Cu.

| $J^{\pi}_n$ | $\pi f_{7/2}$ | $\pi p_{3/2}$ | $\pi f_{5/2}$ | $\pi p_{1/2}$ | $\pi g_{9/2}$ | $\pi d_{5/2}$ |
|---|---|---|---|---|---|---|
| $1/2^-$ | 7.61 | 0.30 | 0.84 | 0.20 | 0.04 | 0.01 |
| $3/2^-$ | 7.67 | 0.88 | 0.35 | 0.05 | 0.05 | 0.01 |
| $5/2^-$ | 7.64 | 0.27 | 0.99 | 0.05 | 0.04 | 0.01 |
| $7/2^-_1$ | 7.65 | 0.76 | 0.48 | 0.05 | 0.05 | 0.01 |
| $7/2^-_2$ | 6.68 | 0.55 | 1.54 | 0.16 | 0.07 | 0.01 |
| $7/2^-_3$ | 7.64 | 0.64 | 0.65 | 0.03 | 0.04 | 0.01 |
| $9/2^-_1$ | 7.66 | 0.25 | 0.99 | 0.05 | 0.04 | 0.01 |
| $9/2^-_2$ | 6.72 | 0.56 | 1.47 | 0.19 | 0.06 | 0.01 |
| $11/2^-$ | 7.70 | 0.66 | 0.55 | 0.03 | 0.05 | 0.01 |
| $13/2^-$ | 7.71 | 0.27 | 0.95 | 0.03 | 0.04 | 0.01 |
| | $\nu f_{7/2}$ | $\nu p_{3/2}$ | $\nu f_{5/2}$ | $\nu p_{1/2}$ | $\nu g_{9/2}$ | $\nu d_{5/2}$ |
| $1/2^-$ | 7.98 | 3.95 | 5.96 | 1.95 | 7.84 | 0.31 |
| $3/2^-$ | 7.98 | 3.93 | 5.93 | 1.93 | 8.02 | 0.21 |
| $5/2^-$ | 7.98 | 3.92 | 5.92 | 1.89 | 8.05 | 0.23 |
| $7/2^-_1$ | 7.99 | 3.96 | 5.97 | 1.97 | 7.87 | 0.24 |
| $7/2^-_2$ | 7.99 | 3.94 | 5.94 | 1.95 | 7.87 | 0.31 |
| $7/2^-_3$ | 7.99 | 3.96 | 5.96 | 1.96 | 7.91 | 0.22 |
| $9/2^-_1$ | 7.99 | 3.97 | 5.97 | 1.97 | 7.86 | 0.24 |
| $9/2^-_2$ | 7.99 | 3.96 | 5.96 | 1.96 | 7.80 | 0.33 |
| $11/2^-$ | 7.99 | 3.98 | 5.99 | 1.98 | 7.88 | 0.19 |
| $13/2^-$ | 7.99 | 3.98 | 5.99 | 1.98 | 7.88 | 0.18 |

be 4.2 W.u., in good agreement with the systematics [9]. For the $3/2^-$ state, the occupation number of the $\pi 2p_{3/2}$ orbital is calculated to be 0.86, increasing to 0.88 in $^{77}$Cu and 1.02 in $^{79}$Cu, in disagreement with the previous calculations of Ref. [4]. The PES of $^{75}$Cu shown in Fig. 7 shows a considerable degree of $\gamma$-softness with a very wide minimum on the prolate side around $Q_0 = 100$ fm$^2$ ($\beta \sim 0.2$), and it is similar to the PES of $^{74}$Ni, shown in Ref. [37].

The systematics of the energies of the first $1/2^-$ states, and the $B(E2; 1/2^- \rightarrow g.s.)$ values in $^{69-79}$Cu are shown in Fig. 8. The $1/2^-$ spin and parity have only been measured in $^{69}$Cu, using transfer reactions [40–42]. The relatively large $B(E2)$ values observed in $^{71-75}$Cu indicate a collective nature of the $1/2^-$ states in these isotopes [9, 19]. In the case of $^{77}$Cu, the $1/2^-$ state was not identified in the $\beta$-decay of $^{77}$Ni [7], which suggests that it lies above the $3/2^-$ state at 293 keV. In $^{75}$Cu, the MCSM finds that the wave function of the $1/2^-$ state is dominated by the $\left|\pi 1f_{5/2} \otimes 2^+_1\right\rangle$ configuration (40%). The calculated $B(E2)$ value agrees very well with the experimental result, and the collectivity is expected to decrease towards the shell closure, with the occupation number of the $\pi 2p_{1/2}$ orbital rapidly increasing from 0.20 in $^{75}$Cu and $^{77}$Cu to 0.62 in $^{79}$Cu. The maximum of collectivity in $^{73,75}$Cu can be interpreted in connection to the fact that the $\nu 1g_{9/2}$ orbital is approximately half-filled, enhancing the occurrence of $\pi 1f_{5/2} - \nu 1g_{9/2}$ quadrupole correlations. As has been discussed in Refs. [7, 20], these correlations account as well for the lowering of the $5/2^-$ state below the $3/2^-$ state in $^{75}$Cu, explaining the change of the ground-state before the calculated cross-

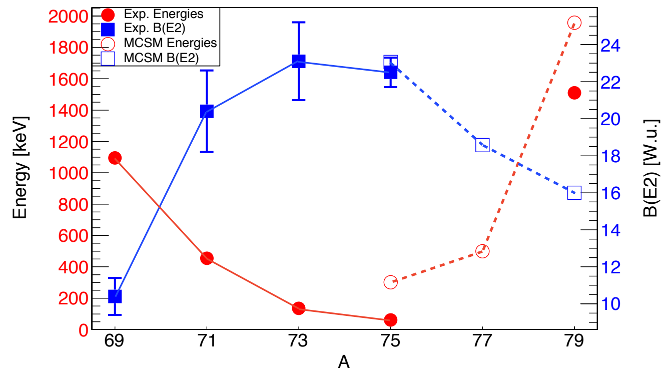


FIG. 8. (Color online) Systematics of the energies of the first $1/2^-$ states (red circles), and $B(E2; 1/2^- \rightarrow g.s.)$ values (blue squares) in odd-A $^{69-79}$Cu isotopes [9, 17, 19]. Results from the MCSM calculations (open symbols) are shown together with experimental values (filled symbols). For $^{79}$Cu, the assignment of the $1/2^-$ state was based on the results of the MCSM calculations (see Ref. [17]).

ing of the $\pi 1f_{5/2}$ and $\pi 2p_{3/2}$ ESPEs in $^{77}$Cu. The $1/2^-$ state is found by the calculations to have an average prolate shape (Fig. 7(a)), in contrast to the $3/2^-$ and the $5/2^-$ states, for which the circles in Figs. 7(b) and (c), respectively, are distributed along the $\gamma$-coordinate. For the $1/2^-$ state, there is also a slight enhancement in occupation of the $\nu d_{5/2}$ orbital, which suggests that $\pi 2f_{1/2} - \nu 2d_{5/2}$ quadrupole correlations play a roll in the collectivity of this state.

### B. Particle-core coupling states.

The systematics of the energies and decay sequences of particle-core coupling states observed in odd-mass $^{69-77}$Cu isotopes are shown in Fig. 9 and Fig. 10, including the results from the $\beta$-decay study of $^{77}$Cu [7] and the results obtained in this work. The $7/2^-$ state at 1871 keV in $^{69}$Cu, is known from transfer [40–42] and multi-nucleon transfer [13] reactions, while the assigned $7/2^-$ states at 1189 and 961 keV in $^{71,73}$Cu, respectively, were identified in the $\beta$-decay study of Ref. [8]. As can be observed in Fig. 9, the energies of these states follow closely the energies of the first $2^+_1$ states of $^{68-72}$Ni. In Ref. [9], Stefanescu *et al.* showed that the $B(E2; 7/2^- \rightarrow 3/2^-)$ values of these states in $^{69,71}$Cu are also very similar to the $B(E2; 2^+_1 \rightarrow 0^+_1)$ values measured in the corresponding $^{68,70}$Ni cores; $^{73}$Cu is the exception, as the measured $B(E2; 7/2^- \rightarrow 3/2^-)$=14.9(18) W.u. [9] is ∼3.5 times larger than the $B(E2; 2^+_1 \rightarrow 0^+_1)$ value measured in $^{72}$Ni [53]. These $7/2^-$ states have been associated with the $\left|\pi 2p_{3/2} \otimes 2^+_1\right\rangle$ configuration [54]. For $^{69,71}$Cu, $\Delta I = 2$ bands have been observed on top of the $7/2^-$ states [11, 13, 14]. The $11/2^-$ members of these bands can be associated with the $\left|\pi 2p_{3/2} \otimes 4^+_1\right\rangle$ configuration.

Two states in $^{75}$Cu were found lying very close to the $2_1^+$ state of $^{74}$Ni. The state at 950 keV decays to both the $3/2^-$ and the $5/2^-$ ground state, and the 884 keV transition to the $3/2^-$ state is 3 times stronger. The state at 992 keV, on the other hand, does not decay to the $3/2^-$ state, but only to the ground state. Based on the systematics shown in Fig. 10, the state at 950 keV is assigned $7/2^-$ spin and parity, and can be associated with the $\left|\pi 2p_{3/2} \otimes 2_1^+\right\rangle$ configuration. The state at 992 keV, which can be associated with the $\left|\pi 1f_{5/2} \otimes 2_1^+\right\rangle$ configuration, is thus assigned $9/2^-$ spin and parity. States at 1726 and 1819 keV were also found very close to the $4_1^+$ state of $^{74}$Ni; the state at 1726 keV decays to the $7/2^-$ state with a transition about 4 times stronger than the transition to the $9/2^-$ state, while the 1819 keV state only decays to the $9/2^-$ state. These two states at 1726 and 1819 keV are thus assigned $11/2^-$ and $13/2^-$ spin and parity, respectively, and could correspond to the $\left|\pi 2p_{3/2} \otimes 4_1^+\right\rangle$ and $\left|\pi 1f_{5/2} \otimes 4_1^+\right\rangle$ configurations, respectively. The energies of the $7/2^-$, $9/2^-$, $11/2^-$ and $13/2^-$ particle-core coupling states are well reproduced by the MCSM (see Fig. 6). The $3/2^-$, $7/2_1^-$ and $11/2^-$ states, as well as the $5/2^-$, $9/2^-$ and $13/2^-$ states, are found to have very similar occupation numbers (see Table II), respectively, supporting their particle-core coupling character. Their average deformation (see Fig. 7) is found to be very similar to that of the $0_1^+$ and $2_1^+$ states of $^{74}$Ni (Ref. [37]). Furthermore, the MCSM calculates $B(E2; 9/2^- \to 5/2^-) =$ 9.6 W.u. and $B(E2; 7/2^- \to 3/2^-) = 8.0$ W.u., values that are very similar to the measured $B(E2; 2_1^+ \to 0_1^+) =$ 7.1(23) W.u. in $^{74}$Ni [50]. An excited state was observed in the experiment at 1680 keV, which only decays directly to the ground state. This state can be associated with the $7/2_3^-$ state found by the MCSM calculations at a very similar energy (see Fig. 6), which is composed by the mixing of several configurations: $\left|\pi 1f_{5/2} \otimes 2_1^+\right\rangle$ (32%), $\left|\pi 1f_{5/2} \otimes 2_2^+\right\rangle$ (27%), $\left|\pi 2p_{3/2} \otimes 4_2^+\right\rangle$ (11%), etc.

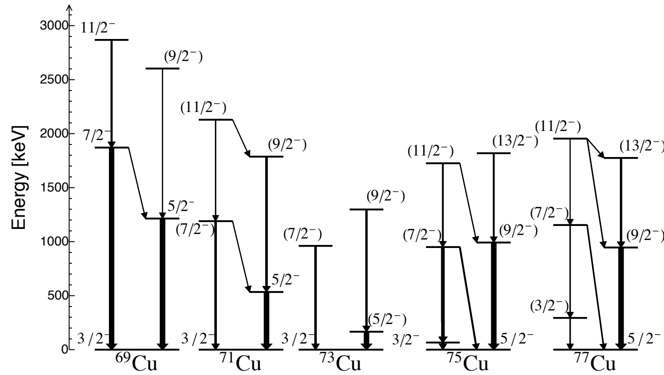


FIG. 10. Systematics of the decay sequences of particle-core coupling states in odd-A $^{69-77}$Cu isotopes [7, 8, 14]. The widths of the transitions correspond with the relative intensities, normalized to the strongest transition shown in each isotope. In $^{71}$Cu, the $11/2^- \to 9/2^-$ transition has only been observed in Ref. [14] and its intensity was normalized according to the observed branching ratio.

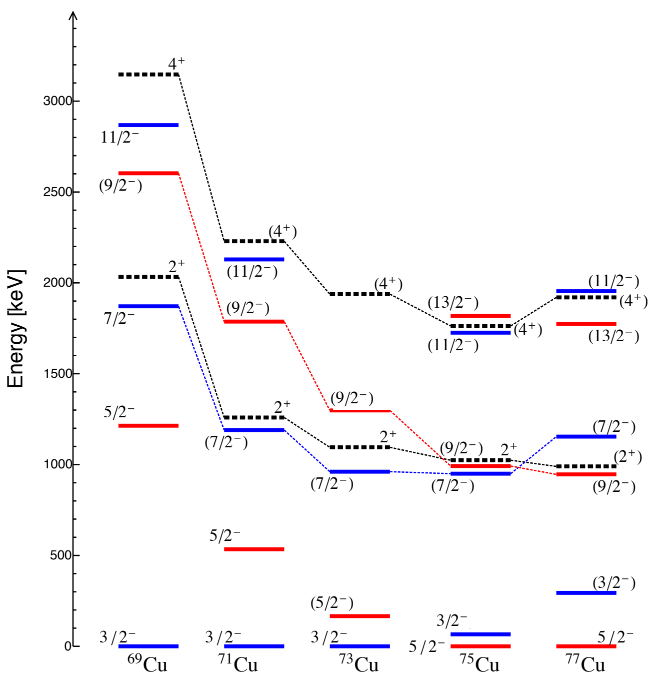


FIG. 9. (Color online) Systematics of the energies of particle-core coupling states in odd-A $^{69-77}$Cu isotopes [7, 8, 14]. The levels corresponding to the Ni cores [44–51] are shown in dashed lines. The $3/2^-$, $7/2^-$ and $11/2^-$ sates (in blue), can be associated with the $\left|\pi 2p_{3/2} \otimes 0_1^+, 2_1^+, 4_1^+\right\rangle$ configurations, respectively, while the $5/2^-$, $9/2^-$ and $13/2^-$ sates (in red) can be associated with the $\left|\pi 1f_{5/2} \otimes 0_1^+, 2_1^+, 4_1^+\right\rangle$ configurations, respectively. In $^{73}$Cu, the spin assignment of the state at 1287 keV is not clear, but the systematics suggest an important $\left|\pi 1f_{5/2} \otimes 2_1^+\right\rangle$ component in its wave function.

The $9/2^-$ $\left|\pi 1f_{5/2} \otimes 2_1^+\right\rangle$ states in $^{69-73}$Cu have not yet been firmly established. In $^{71}$Cu, a state at 1786 keV was first observed in fragmentation [11] and multi-nucleon transfer reactions [12], and a $9/2^+$ spin and parity was proposed in the latter work; afterwards, Franchoo *et al.* [8] proposed a $\left|\pi 1f_{5/2} \otimes 2_1^+\right\rangle$ configuration for this state, together with another possible member of the same multiplet observed at 1846 keV, but the proposed $9/2^-$ and $7/2^-$ spins and parities for these two states were not unambiguously assigned. Later, in another multi-nucleon transfer experiment [14], the state at 1786 keV was found to be connected with the $11/2^-$ $\left|\pi 2p_{3/2} \otimes 4_1^+\right\rangle$ state (as shown in Fig. 10) and assigned a $9/2^-$ spin and parity. For $^{69}$Cu, in the $\beta$-decay experiment of Ref. [8], a $9/2^-$ state was proposed at 2603 keV, but it was suggested to have a different configuration based on the comparison with the shell-model calculations presented in Ref. [13]. In $^{73}$Cu, Franchoo *et al.* [8] proposed the observed state at 1297 keV to have a $\left|\pi 1f_{5/2} \otimes 2_1^+\right\rangle$ configuration, with possible $9/2^-$ or $7/2^-$ spins and parity; however, a very low $B(E2)$ value measured later for its decay to the $5/2^-$ state (< 2 W.u.), and the comparison with shell model calculations suggested a $5/2^-$ spin and parity assignment for this state, and a mixed $|\pi 1f_{5/2} \otimes 0_1^+, 2_1^+\rangle$ configuration [10]. These states have been included in Figs. 9 and 10, and the observed trend in their energies, very similar to the trend followed by the $5/2^-$ sates, together with their decay patterns, suggest an important $|\pi 1f_{5/2} \otimes 2_1^+\rangle$ component in their wave functions. In the case of $^{73}$Cu, the relatively long lifetime measured for this state in Ref. [10] could be related to unaccounted side feeding from long-lived states.

### C. The intruder band.

In $^{69-73}$Cu, other $7/2^-$ states have been observed at 1711, 981, and 1010 keV, respectively [8], lying very close to the $7/2^-$ particle-core coupling states. While for the latter, the $B(E2; 7/2^- \to 3/2^-)$ values rapidly increase from 4.6(7) W.u. in $^{69}$Cu to 14.9(18) W.u. in $^{73}$Cu [9], low $B(E2; 7/2^- \to 3/2^-)$ values ($< 3$ W.u.) have been measured in $^{69,71}$Cu for the $7/2^-$ "intruder" states [10]. These intruder states have been associated with a $1f_{7/2}^{-1}$ proton-hole configuration [54]. In $^{69}$Cu, the $7/2^-$ state at 1711 keV was found, in transfer reactions [40, 42], to contain around one third of the $\pi 1f_{7/2}^{-1}$ strength, with a $C^2S$ about 5 times larger than that of the $7/2^-$ particle-core coupling state. However, a similar experiment performed for $^{71}$Cu did not find any significant part of the $\pi 1f_{7/2}^{-1}$ strength below 2 MeV, questioning the proton-hole character of the 981 keV state. In $^{69,71}$Cu, $\Delta I = 1$ bands have been observed on top of the $7/2^-$ intruder states, using multi-nucleon transfer reactions [13–15]. In $^{73}$Cu, the state at 1489 keV was assigned $9/2^-$ spin and parity, and proposed to be a member of the $\pi 1f_{7/2}^{-1}$ intruder band [8]. In $^{77}$Cu, the $7/2^-$ intruder state at 2068 keV was first observed in the $\beta$-decay of $^{77}$Ni [7], and the assignment was based on the results of the MCSM calculations, which found the state to be dominated by a seven proton occupancy in the $\pi 1f_{7/2}$ orbital (74%). This state was later strongly populated in the proton knockout experiment of Ref. [16], supporting it's $1f_{7/2}^{-1}$ proton-hole character. In the proton knockout experiment of Ref. [17], none of the populated states in $^{79}$Cu was identified to contain a large fraction of the $\pi 1f_{7/2}^{-1}$ strength.

The systematics of the $7/2^-$ intruder states in $^{69-77}$Cu and the band members up to spin $11/2^-$ are shown in Fig. 11a. In the present work, the excited states at 1484, 1989, and 2516 keV in $^{75}$Cu are assigned, respectively, $7/2^-$, $9/2^-$ and $11/2^-$ spins and parities, and are proposed to be members of the $\pi 1f_{7/2}^{-1}$ intruder band. The assignment is based on the similarity of the observed decay sequence with the $9/2^- \to 7/2^-$ and the $11/2^- \to 9/2^-$ transitions in $^{69-73}$Cu and the comparison with the MCSM values (see Fig. 6). The proton-hole character of the 1484 and 2068 keV states in $^{75}$Cu and $^{77}$Cu, respectively, has been now confirmed in the proton knockout experiment of Ref [21].

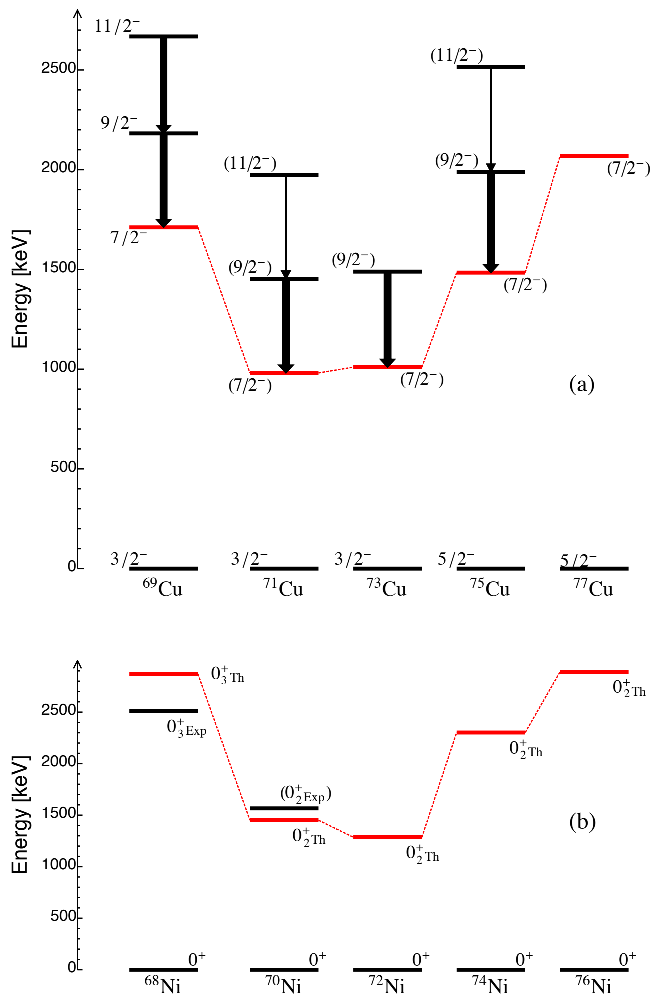


FIG. 11. (Color online) (a) Systematics of the intruder states in odd-A $^{69-77}$Cu isotopes. The widths of the $11/2^- \to 9/2^-$ transitions are normalized to those of the $9/2^- \to 7/2^-$ transitions in each isotope. The relative intensities were taken from the $\beta$-decay experiment of Ref. [8], except for $^{69}$Cu, where the $11/2^-$ state has only been seen in Ref. [13]. (b) Intruder $0^+$ states in the corresponding Ni cores. The experimental $0^+_{\rm Exp}$ states in $^{68,70}$Ni are those in Refs. [44, 46]. The MCSM values of the $0^+_{\rm Th}$ energies have been previously presented in Ref. [37].

The $\pi 1f_{7/2}^{-1}$ intruder states in odd-mass Cu isotopes with $N \geq 40$, have been suggested to be formed by the coupling of one proton in the $\pi 1f_{7/2}$ orbital to excited $0^+$ states in the corresponding even-even Ni cores [15]. These excited $0^+$ states are expected to have a prolate shape, originated by the promotion of two protons from the $\pi 1f_{7/2}$ orbital across the $Z = 28$ shell gap [37, 52]. In $^{75}$Cu, the MCSM calculations find the occupation number of the $\pi 1f_{7/2}$ orbital to be 6.71 for the $7/2_2^-$ intruder state, and similar values are found for the corresponding states in $^{77}$Cu and $^{79}$Cu: 6.68 and 6.82, respectively. This state is found by the calculations to be prolate, with an average deformation of $\beta \sim 0.27$

(see Fig. 7). The collectivity of the intruder band is expected to be large; for $^{77}$Cu, the MCSM calculations find $B(E2, 9/2^- \rightarrow 7/2^-) = 34$ W.u. The calculated energies of the prolate $0^+$ states in the even-even $^{68-76}$Ni isotopes are shown in Fig. 11b. Candidates for these yrare $0^+$ states and their $2^+$ and $4^+$ band members have been proposed in $^{68}$Ni [44, 45, 52, 55] and $^{70}$Ni [46, 47, 56]. In $^{72}$Ni, two sates observed at 2010 and 2320 keV were suggested to be possible prolate intruder states [57], as well as in $^{76}$Ni, for an observed state at 2995 keV [51].

The MCSM calculations explain the presence of the prolate, deformed bands at relatively low energies at $N \sim 42, 44$ as an effect of the Type II shell evolution [37, 38]. While the $\nu 1g_{9/2}$ orbital is expected to follow a normal filling in the ground-state bands of the $38 \leq N \leq 48$, even-even Ni isotopes with a maximum of collectivity at $N \sim 44, 46$ [53] (where the $\nu 1g_{9/2}$ orbital can thus be expected to be half filled), the addition of two protons from the $1f_{7/2}$ orbital to the $pf$ shell favors the occurrences of $\pi 1f_{5/2} - \nu 1g_{9/2}$ quadrupole correlations and precipitates the filling of the $\nu 1g_{9/2}$ orbital in the intruder band, reaching half of the total occupancy at $N \sim 42, 44$. For Ni isotopes with $N > 44$, the Type II shell evolution is suppressed because of the increasing occupancy of the the $\nu 1g_{9/2}$ orbital, therefore, the deformation of the prolate band decreases and the energy of the prolate $0^+$ state is expected to increase gradually from $^{72}$Ni to $^{76}$Ni. As can be seen in Fig. 11, the intruder states in odd-mass $^{69-77}$Cu isotopes follow a parabolic trend very similar to the predicted one for the yrare, prolate $0^+$ states in the $^{68-76}$Ni isotopes. The asymmetry of the parabola can be understood as an effect of the Type I shell evolution [37, 38]: the energy of the $7/2^-$ intruder state in $^{75}$Cu is lower than the energy of the corresponding $7/2^-$ state in $^{69}$Cu because of reduction of the $\pi 1f_{7/2} - \pi 1f_{5/2}$ single-particle gap under the influence of the monopole component of the nucleon-nucleon interaction [2, 3].

## V. SUMMARY AND CONCLUSIONS

Excited states in $^{75}$Cu up to $\sim 4$ MeV were populated in the $\beta$-decay of $^{75}$Ni. The $^{75}$Ni nuclei were produced at the RIBF in RIKEN, in the in-flight fission of $345A$ MeV $^{238}$U projectiles on a $^{9}$Be target. The fragments were selected and identified in the BigRIPS fragment separator and later implanted in a stack of DSSSDs for the detection of the $\beta$-decay electrons. The EURICA array of HPGe cluster detectors was used for the detection of the $\beta$-delayed $\gamma$-rays. A level scheme was proposed based on the $\gamma$-$\gamma$ coincidence analysis, from which the location of the two previously known low-lying isomeric states was clarified. MCSM calculations were performed on the $pfg_{9/2}d_{5/2}$ model space for both neutrons and protons, using the A3DA interaction. The level structure below 2 MeV was interpreted based on the results of the shell model calculations and the systematics of odd-A Cu isotopes with $N \geq 40$ and their corresponding even-even Ni cores. Different single-particle, core-coupling, and intruder states were proposed, and spins and parities were assigned for these states. The remaining states shown in the level scheme of Fig. 5 are less straight forward to interpret and probably highly mixed in their wave functions. In the light of the new experimental information presented in this work, together with the recent results in $^{77}$Cu [7] and $^{79}$Cu [17], the evolution of the low-lying states in $^{69-79}$Cu was discussed.

## ACKNOWLEDGMENTS

This work was carried out at the RIBF operated by RIKEN Nishina Center, RIKEN and CNS, University of Tokyo. The research leading to the results has received funding from the Research Council of Norway under project Grants No. 240104 and No. 213442 and from KAKENHI (under Grants No. 25247045, No. 23.01752, and No. 25800130); U.S. DOE Grant No. DE-FG02-91ER-40609; Spanish Ministerio de Ciencia e Innovación Contracts No. FPA2009-13377C02 and No. FPA2011-29854-C04; and the Hungarian Scientific Research Fund OTKA Contract No. K100835. The Monte Carlo shell model calculations were performed on K computer at RIKEN AICS (hp140210, hp150224, hp160211). This work was supported in part by the HPCI Strategic Program (The Origin of Matter and the Universe), by "Priority Issue on Post-K computer" (Elucidation of the Fundamental Laws and Evolution of the Universe) (hp160211), and by CNS-RIKEN joint project for large-scale nuclear structure calculations. The authors acknowledge the EUROBALL Owners Committee for the loan of germanium detectors and the PreSpec Collaboration for the readout electronics of the cluster detectors. Part of the WAS3ABi has been supported by the Rare Isotope Science Project which is funded by the Ministry of Education, Science and Technology (MEST) and National Research Foundation (NRF) of Korea.

[1] O. Sorlin and M.-G. Porquet, Prog. Part. Nucl. Phys. **61** 602 (2008).
[2] T. Otsuka *et al.*, Phys. Rev. Lett. **104**, 012501 (2010).
[3] T. Otsuka, Phys. Scr. T **152**, 014007 (2013).
[4] K. Sieja and F. Nowacki, Phys. Rev. C **81**, 061303(R) (2010).
[5] K. T. Flanagan *et al.*, Phys. Rev. Lett. **103**, 142501 (2009).
[6] U. Köster *et al.*, Phys. Rev. C **84**, 034320 (2011).
[7] E. Sahin *et al.*, Phys. Rev. Lett. **118**, 242502 (2017).
[8] S. Franchoo *et al.*, Phys. Rev. C **64**, 054308 (2001).
[9] I. Stefanescu *et al.*, Phys. Rev. Lett. **100**, 112502 (2008).

[10] E. Sahin *et al.*, Phys. Rev. C **91**, 034302 (2015).
[11] R. Grzywacz *et al.*, Phys. Rev. Lett. **81**, 766 (1998).
[12] T. Ishii *et al.*, Phys. Rev. Lett. **81**, 4100 (1998).
[13] T. Ishii *et al.*, Phys. Rev. Lett. **84**, 39 (2000).
[14] I. Stefanescu *et al.*, Phys. Rev. C **79**, 034319 (2009).
[15] S. N. Liddick *et al.*, Phys. Rev. C **92**, 024319 (2015).
[16] Zs. Vajta *et al.*, Phys. Lett. B **782**, 99 (2018).
[17] L. Olivier *et al.*, Phys. Rev. Lett. **119**, 192501 (2017).
[18] J. M. Daugas *et al.*, Phys. Rev. C **81**, 034304 (2010).
[19] C. Petrone *at al.*, Phys. Rev. C **94**, 024319 (2016).
[20] Y. Ichikawa *at al.*, Nature Physics **15**, 321 (2019).
[21] E. Sahin *et al.*, to be submitted.
[22] P.-A. Söderström *et al.*, Nucl. Instr. Meth B **317**, 649-652 (2013).
[23] T. Motobayashi, H. Sakurai, Prog. Theor. Exp. Phys. **2012**, 03C001.
[24] H. Okuno, N. Fukunishi, and O. Kamigaito Prog. Theor. Exp. Phys. **2012**, 03C002.
[25] T. Kubo *et al.*, Prog. Theor. Exp. Phys. **2012**, 03C003.
[26] J. P. Dufour *et al.*, Nucl. Instr. Meth A **248**, 267 (1986).
[27] Z. Y. Xu, Ph.D. thesis, Department of Physics, University of Tokyo (2014). http://hdl.handle.net/2261/57714
[28] N. Fukuda *et al.*, Nucl. Instr. Meth. B **317**, 323-332 (2013).
[29] Z. Y. Xu *et al.*, Phys. Rev. Lett. **113**, 032505 (2014).
[30] S. Nishimura, Prog. Theor. Exp. Phys. **2012**, 03C006.
[31] P. Hosmer *et al.*, Phys. Rev. C **82**, 025806 (2010).
[32] The Evaluated Nuclear Structure Data File, ENSDF. http://www.nndc.bnl.gov/ensdf/
[33] BrIcc, Conversion Coefficient Calculator. http://bricc.anu.edu.au
[34] M. Wang *et al.*, Chin. Phys. C, 1603 (2012).
[35] C. J. Chiara *et al.*, Phys. Rev. C **85**, 024309 (2012).
[36] T. Otsuka *et al.*, Phys. Rev. Lett. **95**, 232502 (2005).
[37] Y. Tsunoda *et al.*, Phys. Rev. C **89**, 031301(R) (2014).
[38] T. Otsuka and Y. Tsunoda, J. Phys. G: Nucl. Part. Phys. **43**, 024009 (2016).
[39] N. Shimizu *et al.*, Prog. Theor. Exp. Phys. 01A205 (2012).
[40] B. Zeidman and J. A. Nolen, Phys. Rev. C **18**, 2122 (1978).
[41] F. Ajzenberg-Selove *et al.*, Phys. Rev. C **24**, 1762 (1981).
[42] P. Morfouace *et al.*, Phys. Rev. C **93**, 064308 (2016).
[43] P. Morfouace *et al.*, Phys. Lett. B **751**, 306 (2015).
[44] F. Recchia *et al.*, Phys. Rev. C **88**, 041302(R) (2013).
[45] F. Flavigny *et al.*, Phys. Rev. C **91**, 034310 (2015).
[46] C. J. Prokop *et al.*, Phys. Rev. C **92**, 061302(R) (2015).
[47] A. I. Morales *et al.*, Phys. Lett. B **765**, 328 (2017).
[48] A. I. Morales *et al.*, Phys. Rev. C **93**, 034328 (2016).
[49] C. Mazzocchi *et al.*, Phys. Lett. B **662**, 45 (2005).
[50] T. Marchi *et al.*, Phys. Rev. Lett. **113**, 182501 (2014).
[51] P.-A. Söderström *et al.*, Phys. Rev. C **92**, 051305(R) (2015).
[52] S. Suchyta *et al.*, Phys. Rev. C **89**, 021301(R) (2014).
[53] K. Kolos *et al.*, Phys. Rev. Lett. **116**, 122502 (2016).
[54] A. M. Oros-Peusquens and P. F. Mantica, Nucl. Phys. A **669**, 81 (2000).
[55] D. Pauwels *et al.*, Phys. Rev. C **82**, 027304 (2010).
[56] C. J. Chiara *et al.*, Phys. Rev. C **91**, 044309 (2015).
[57] W. B. Walters *et al.*, AIP Conference Proceedings **1681**, 030007 (2015).